nature COMMUNICATIONS

ARTICLE

Received 2 Jul 2012 | Accepted 23 Nov 2012 | Published 8 Jan 2013

DOI: 10.1038/ncomms2327

Sulphur–TiO_2 yolk–shell nanoarchitecture with internal void space for long-cycle lithium–sulphur batteries

Zhi Wei Seh[1,*], Weiyang Li[1,*], Judy J. Cha[1], Guangyuan Zheng[2], Yuan Yang[1], Matthew T. McDowell[1], Po-Chun Hsu[1] & Yi Cui[1,3]

Sulphur is an attractive cathode material with a high specific capacity of 1,673 mAh g^{-1}, but its rapid capacity decay owing to polysulphide dissolution presents a significant technical challenge. Despite much efforts in encapsulating sulphur particles with conducting materials to limit polysulphide dissolution, relatively little emphasis has been placed on dealing with the volumetric expansion of sulphur during lithiation, which will lead to cracking and fracture of the protective shell. Here, we demonstrate the design of a sulphur–TiO_2 yolk–shell nanoarchitecture with internal void space to accommodate the volume expansion of sulphur, resulting in an intact TiO_2 shell to minimize polysulphide dissolution. An initial specific capacity of 1,030 mAh g^{-1} at 0.5 C and Coulombic efficiency of 98.4% over 1,000 cycles are achieved. Most importantly, the capacity decay after 1,000 cycles is as small as 0.033% per cycle, which represents the best performance for long-cycle lithium–sulphur batteries so far.

[1] Department of Material Science and Engineering, Stanford University, Stanford, California 94305, USA. [2] Department of Chemical Engineering, Stanford University, Stanford, California 94305, USA. [3] Stanford Institute for Materials and Energy Science, SLAC National Accelerator Laboratory, Menlo Park, California 94025, USA. * These authors contributed equally to this work. Correspondence and requests for materials should be addressed to Y.C. (email: yicui@stanford.edu).

There has been a steady increase in the demand for high-performance and long-lasting rechargeable batteries for a wide range of applications, ranging from portable electronics and consumer devices to electric vehicles and large-scale grid energy storage[1–9]. Unfortunately, the energy density and cycle life of existing lithium-ion batteries remain insufficient for many of the aforementioned applications, prompting the urgent need for new electrode materials with much higher charge capacities[1–5]. Over the years, significant progress has been made in the development of new high-performance anode materials (such as silicon and tin) for rechargeable batteries[10–14], but the major limiting factor is still the relatively low capacity of cathodes. Sulphur is a promising cathode material with a theoretical specific capacity of 1,673 mAh g^{-1}, which is ~5 times that of existing materials based on transition metal oxides and phosphates[15–18]. However, many challenges remain in developing a practical lithium–sulphur battery for commercialization. It is known that sulphur particles suffer from the problems of (a) poor electronic conductivity, (b) dissolution of intermediate polysulphides and (c) large volumetric expansion (~80%) upon lithiation, which results in rapid capacity decay and low Coulombic efficiency (Fig. 1a)[15–18]. Over the years, extensive efforts have been devoted to addressing the first two problems, by encapsulating sulphur particles with conducting materials, including porous carbon[19–27], graphene oxide[28,29] and conductive polymers[30–33], in an attempt to improve their electronic conductivity and limit polysulphide dissolution. However, insufficient emphasis has been placed on dealing with the third challenge—the large volumetric expansion of sulphur during lithiation coupled with polysulphide dissolution. This poses a critical problem because volume expansion of the sulphur core will cause the protective coating layer to crack and fracture, rendering the conventional core–shell morphology[32–35] ineffective in trapping polysulphides (Fig. 1b). In this respect, the strategy of adjusting the amount of sulphur infusion into mesoporous carbon has been demonstrated[20,23], but it can be difficult to control the uniformity of sulphur filling within the pores of each particle and across different particles. Overall, the long-term cycling performance for lithium–sulphur batteries remains to be improved.

Herein, we demonstrate for the first time, the design of a sulphur–TiO_2 yolk–shell nanoarchitecture for stable and prolonged cycling over 1,000 charge/discharge cycles in lithium–sulphur batteries. The unique advantage of the yolk–shell morphology lies in the presence of internal void space to accommodate the large volumetric expansion of sulphur during lithiation, thus preserving the structural integrity of the shell to minimize polysulphide dissolution (Fig. 1c). In comparison with bare sulphur and sulphur–TiO_2 core–shell nanoparticles, the yolk–shell nanostructures are found to exhibit the highest capacity retention owing to the effectiveness of the intact TiO_2 shell in limiting polysulphide dissolution. Using the yolk–shell nanoarchitecture, an initial specific capacity of 1,030 mAh g^{-1} at 0.5 C and Coulombic efficiency of 98.4% over 1,000 cycles is achieved. Most importantly, the capacity decay at the end of 1,000 cycles is found to be as small as 0.033% per cycle (3.3% per 100 cycles). To the best of our knowledge, this is the first time that a lithium–sulphur battery with this level of performance has been described.

Results

Synthesis of the sulphur–TiO_2 yolk–shell nanostructures. The sulphur–TiO_2 yolk–shell morphology was experimentally realized as shown schematically in Fig. 2a. First, monodisperse sulphur nanoparticles were prepared using the reaction of sodium thiosulfate with hydrochloric acid (Supplementary Fig. S1). The sulphur nanoparticles were then coated with TiO_2 through controlled hydrolysis of a sol-gel precursor, titanium diisopropoxide bis(acetylacetonate), in an alkaline isopropanol/aqueous

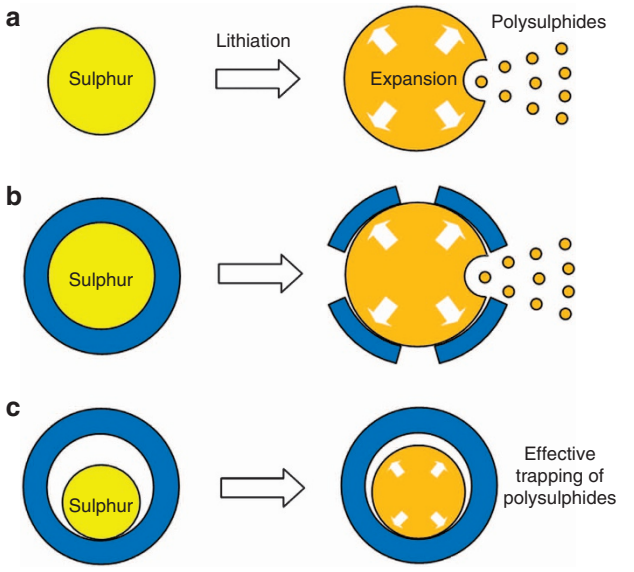

Figure 1 | Schematic of the lithiation process in various sulphur-based nanostructure morphologies. (**a**) Bare sulphur particles undergo large volumetric expansion and polysulphide dissolution upon lithiation, resulting in rapid capacity decay and low Coulombic efficiency. (**b**) Although the core–shell morphology provides a protective coating, cracking of the shell will occur upon volume expansion of sulphur during lithiation, leading to polysulphide dissolution as well. (**c**) The yolk–shell morphology provides internal void space to accommodate the volume expansion of sulphur during lithiation, resulting in a structurally intact shell for effective trapping of polysulphides.

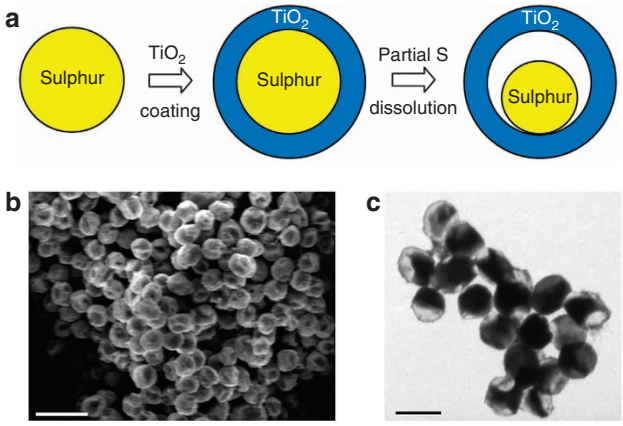

Figure 2 | Synthesis and characterization of sulphur–TiO_2 yolk–shell nanostructures. (**a**) Schematic of the synthetic process that involves coating of sulphur nanoparticles with TiO_2 to form sulphur–TiO_2 core–shell nanostructures, followed by partial dissolution of sulphur in toluene to achieve the yolk–shell morphology. (**b**) SEM image and (**c**) TEM image of as-synthesized sulphur–TiO_2 yolk–shell nanostructures. (**b**) Scale bar, 2 μm. (**c**) Scale bar, 1 μm. Through large-ensemble measurements, the average nanoparticle size and TiO_2 shell thickness were determined to be 800 and 15 nm, respectively.

solution, resulting in the formation of sulphur–TiO_2 core–shell nanoparticles (Supplementary Fig. S2; the transmission electron microscopy (TEM) image was taken immediately after the electron beam was turned on to avoid sublimation of sulphur under the beam). This was followed by partial dissolution of sulphur in toluene to create an empty space between the sulphur core and the TiO_2 shell, resulting in the yolk–shell morphology. The scanning electron microscopy (SEM) image in Fig. 2b shows uniform spherical nanoparticles of ~800 nm in size. The TEM image in Fig. 2c, taken immediately after the electron beam was turned on, shows sulphur nanoparticles encapsulated within TiO_2 shells (~15 nm thick) with internal void space. Owing to the two-dimensional projection nature of TEM images, the void space will appear as either an empty area or an area of lower intensity depending on the orientation of the particles (Fig. 2c). The TiO_2 in the yolk–shell nanostructures were determined to be amorphous using X-ray diffraction (Supplementary Fig. S3). The ability of toluene to diffuse through the TiO_2 shell to partially dissolve sulphur indicates its porous nature, which is typical of amorphous TiO_2 prepared using sol-gel methods[36]. The average pore diameter was determined to be ~3 nm using the Barrett–Joyner–Halenda method, which corresponds to a mesoporous structure.

Volume expansion in the yolk–shell nanostructures. Next, we investigated the effectiveness of the yolk–shell morphology in accommodating the volume expansion of sulphur and limiting polysulphide dissolution. The sulphur–TiO_2 yolk–shell nanostructures were drop-cast onto conducting carbon paper to form working electrodes, and pouch cells were assembled using lithium foil as the counter electrode. The cells were discharged at 0.1 C (1 C = 1,673 mA g^{-1}) to a voltage of 1.7 V versus Li^+/Li, during which a capacity of 1,110 mAh g^{-1} was attained (Supplementary Fig. S4), and the voltage was maintained for over 20 h. The as-obtained discharge profile shows the typical two-plateau behaviour of sulphur cathodes, indicating the conversion of elemental sulphur to long-chain lithium polysulphides (Li_2S_n, $4 \leq n \leq 8$) at ~2.3 V, and the subsequent formation of Li_2S_2 and Li_2S at ~2.1 V (Supplementary Fig. S4)[15–18]. After the discharge process, the contents of the cells (cathode, anode and separator) were washed with 1,3-dioxolane (DOL) solution for further characterization. This polysulphide-containing solution was then oxidized with concentrated HNO_3 and diluted with deionized water for analysis of sulphur content using inductively coupled plasma (ICP) spectroscopy[37]. For comparison, electrode materials were also prepared using the bare sulphur and sulphur–TiO_2 core–shell nanoparticles and subject to the same treatment.

There was little change in the morphology and size distribution of the sulphur–TiO_2 yolk–shell nanostructures before and after lithiation (Fig. 3a–c). TEM image of a lithiated yolk–shell nanostructure shows a structurally intact TiO_2 coating (Fig. 3d), indicating the ability of the yolk–shell design in accommodating the volume expansion of sulphur. The presence of lithiated sulphur and TiO_2 in the yolk–shell nanostructure was confirmed using energy-dispersive X-ray spectroscopy and electron energy loss spectroscopy (Fig. 3e). In the case of bare sulphur and sulphur–TiO_2 core–shell nanoparticles, random precipitation of irregularly shaped Li_2S_2 and Li_2S particles was observed on the electrodes owing to dissolution of lithium polysulphides into the electrolyte (Supplementary Fig. S5)[15–18]. ICP analysis performed on the contents of the discharged cells showed a loss of 81 and 62% of the total sulphur mass into the electrolyte for the bare sulphur and sulphur–TiO_2 core–shell nanoparticles, respectively. In comparison, only 19% of the total sulphur mass was found to be dissolved in the electrolyte in the case of the yolk–shell nanostructures, which indicates the effectiveness of the intact TiO_2 shell in limiting polysulphide dissolution.

Electrochemical performance. To further evaluate the electrochemical cycling performance of the sulphur–TiO_2 yolk–shell nanoarchitecture, 2,032-type coin cells were fabricated. The working electrodes were prepared by mixing the yolk–shell nanostructures with conductive carbon black and polyvinylidene fluoride binder in *N*-methyl-2-pyrrolidinone to form a slurry, which was then coated onto aluminium foil and dried under

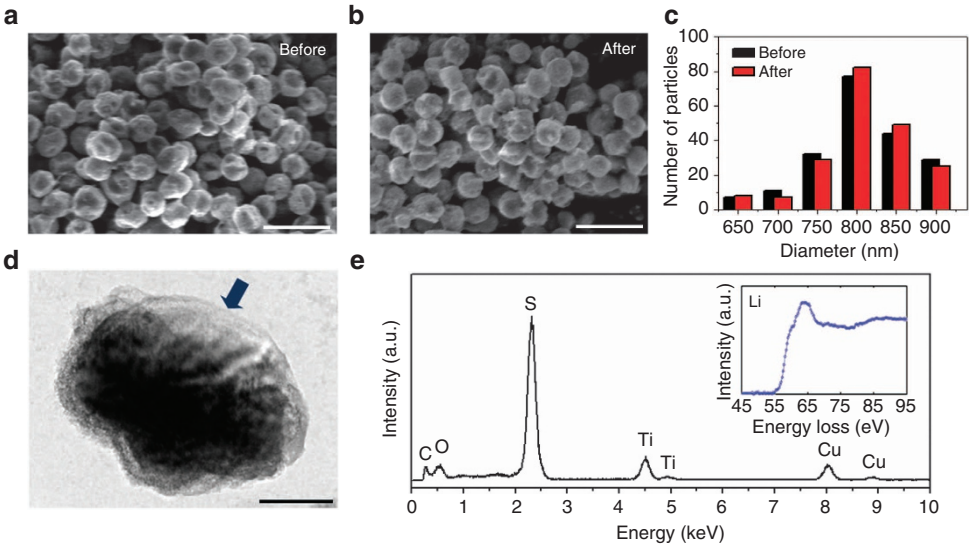

Figure 3 | Morphology of sulphur–TiO_2 yolk–shell nanostructures after lithiation. (**a**–**c**) SEM images of sulphur–TiO_2 yolk–shell nanostructures (**a**) before and (**b**) after lithiation and (**c**) their respective particle size distributions. (**a**,**b**) Scale bar, 2 μm. (**d**) TEM image of a sulphur–TiO_2 yolk–shell nanostructure after lithiation, showing the presence of an intact TiO_2 shell (highlighted by arrow). Scale bar, 200 nm. (**e**) Energy-dispersive X-ray spectrum and electron energy loss spectrum (inset) of the nanostructure in (**d**), showing the presence of lithiated sulphur and TiO_2. The Cu peak arises owing to the use of a copper TEM grid.

vacuum. Using lithium foil as the counter electrode, the cells were cycled from 1.7–2.6 V versus Li^+/Li. The electrolyte used was lithium bis(trifluoromethanesulfonyl)imide in 1,2-dimethoxyethane and 1,3-DOL, with $LiNO_3$ (1 wt%) as an additive to help passivate the surface of the lithium anode and reduce the shuttle effect[17,18]. Specific capacity values were calculated based on the mass of sulphur, which was determined using thermogravimetric analysis (Supplementary Fig. S6). The sulphur content was found to be ~71 wt% in the yolk–shell nanostructures, accounting for ~53 wt% of the electrode mix, with a typical sulphur mass loading of 0.4–0.6 mg cm^{-2}. The contribution of TiO_2 to the total capacity is very small in the voltage range used in our work[38,39].

The sulphur–TiO_2 yolk–shell nanoarchitecture exhibited stable cycling performance over 1,000 charge/discharge cycles at 0.5 C (1 C = 1,673 mA g^{-1}) as displayed in Fig. 4a (see also Supplementary Fig. S7). After an initial discharge capacity of 1,030 mAh g^{-1}, the yolk–shell nanostructures achieved capacity retentions of 88, 87 and 81% at the end of 100, 200 and 500 cycles, respectively (Fig. 4a,b). Most importantly, after prolonged cycling over 1,000 cycles, the capacity retention was found to be 67%, which corresponds to a very small capacity decay of 0.033% per cycle (3.3% per 100 cycles), representing the best performance for long-cycle lithium–sulphur batteries so far. The average Coulombic efficiency over 1,000 cycles was calculated to be 98.4%, which shows little shuttle effect owing to polysulphide dissolution. In comparison, cells based on bare sulphur and sulphur–TiO_2 core–shell nanoparticles suffered from rapid capacity decay, showing capacity retentions of 48 and 66%, respectively, after only 200 cycles (Fig. 4b), indicating a greater degree of polysulphide dissolution into the electrolyte.

Next, the sulphur–TiO_2 yolk–shell nanostructures were subject to cycling at various C-rates to evaluate their robustness (Fig. 4c,d). After an initial discharge capacity of 1,215 mAh g^{-1} at 0.2 C, the capacity was found to stabilize at 1,010 mAh g^{-1}. Further cycling at 0.5, 1 and 2 C showed high reversible capacities of 810, 725 and 630 mAh g^{-1}, respectively (Fig. 4c,d). When the C-rate was switched abruptly from 2 to 0.2 C again, the original capacity was largely recovered (Fig. 4c), indicating robustness and stability of the cathode material. Moreover, there was little change in the thickness of the cathode before and after 70 cycles at these various C-rates (Supplementary Fig. S8), which further confirms the ability of the yolk–shell nanostructures in accommodating the volume expansion of sulphur.

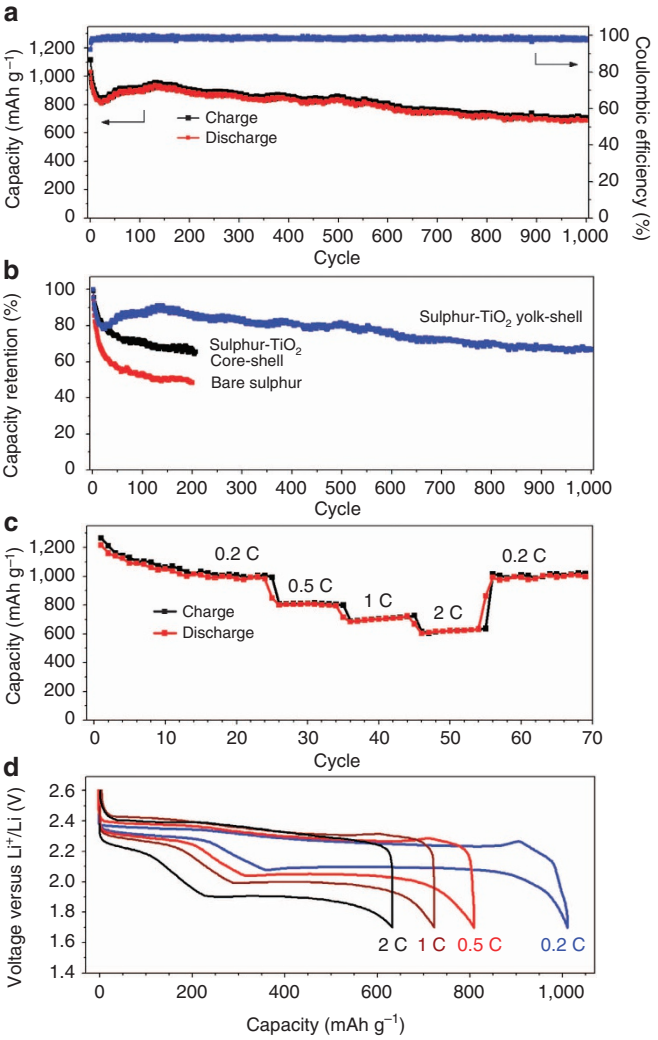

Figure 4 | Electrochemical performance of sulphur–TiO_2 yolk–shell nanostructures. (**a**) Charge/discharge capacity and Coulombic efficiency over 1,000 cycles at 0.5 C. (**b**) Capacity retention of sulphur–TiO_2 yolk–shell nanostructures cycled at 0.5 C, in comparison with bare sulphur and sulphur–TiO_2 core–shell nanoparticles. (**c**) Charge/discharge capacity and (**d**) voltage profiles of sulphur–TiO_2 yolk–shell nanostructures cycled at various C-rates from 0.2 to 2 C. Specific capacity values were calculated based on the mass of sulphur.

Discussion

There are two important characteristics of such a yolk–shell design that imparts the sulphur–TiO_2 nanostructures with stable cycling performance over 1,000 charge/discharge cycles. First, sufficient empty space was present to allow for volume expansion of sulphur. Using image processing software on the yolk–shell nanostructures (Fig. 2c), sulphur was determined to occupy ~62% of the volume within the TiO_2 shell, which corresponds to 38% internal void space. This value is supported by thermogravimetric analysis of the relative wt% of sulphur versus TiO_2 (Supplementary Fig. S6), from which the volume of empty space in the yolk–shell nanostructures was estimated to be 37%. This volume of void space can accommodate ~60% volume expansion of the sulphur present within the shell, allowing for 1,250 mAh g^{-1}, that is, 75% of the maximum theoretical capacity of sulphur, to be utilized (assuming volume expansion is linearly dependent on the degree of lithiation). Experimentally, we have been able to achieve a maximum discharge capacity of 1,215 mAh g^{-1} (Fig. 4c), therefore there is sufficient void space for volume expansion without causing the shell to crack and fracture. Second, the intact TiO_2 shell, with its small pore size of ~3 nm, was effective in minimizing polysulphide dissolution. Mesoporous structures, such as those based on carbon, have been shown to help trap polysulphides owing to their small pore sizes (~3 nm)[20,27]. Moreover, metal oxides such as TiO_2 possess hydrophilic Ti–O groups and surface hydroxyl groups, which are known to bind favourably with polysulphide anions, hence further limiting the extent of polysulphide dissolution[21,40].

In conclusion, we have demonstrated for the first time, the design of a sulphur–TiO_2 yolk–shell nanoarchitecture for long cycling capability over 1,000 charge/discharge cycles, with a capacity decay as small as 0.033% per cycle. Compared with its bare sulphur and sulphur–TiO_2 core–shell counterparts, the yolk–shell nanostructures exhibited the highest capacity retention owing to the presence of internal void space to accommodate the volume expansion of sulphur during lithiation, resulting in an intact shell to minimize polysulphide dissolution. Insight gained

from this work can be applied to other high-capacity anode and cathode material systems, especially those that undergo large volumetric expansion, providing new avenues for the future development of high-performance rechargeable batteries.

Methods

Synthesis of sulphur–TiO_2 yolk–shell nanostructures. First, sulphur nanoparticles were synthesized by adding concentrated HCl (0.8 ml, 10 M) to an aqueous solution of $Na_2S_2O_3$ (100 ml, 0.04 M) containing a low concentration of polyvinylpyrrolidone (PVP, $M_w \sim 55{,}000$, 0.02 wt%; we note that at much higher PVP concentrations, hollow sulphur particles are formed instead). After reaction for 2 h, the sulphur nanoparticles (100 ml) were washed by centrifugation and redispersed into an aqueous solution of PVP (20 ml, 0.05 wt%). For TiO_2 coating, the solution of sulphur nanoparticles (20 ml) was mixed with isopropanol (80 ml) and concentrated ammonia (2 ml, 28 wt%). Titanium diisopropoxide bis(acetylacetonate) (50 ml, 0.01 M in isopropanol) was then added in five portions (5×10 ml) at half hour intervals. After reaction for 4 h, the solution of sulphur–TiO_2 core–shell nanoparticles was washed by centrifugation to remove freely hydrolysed TiO_2, followed by redispersion into deionized water (20 ml). To prepare the sulphur–TiO_2 yolk–shell nanostructures, the solution of core–shell particles (20 ml) was stirred with isopropanol (20 ml) and toluene (0.4 ml) for 4 h to achieve partial dissolution of sulphur. The as-synthesized sulphur–TiO_2 yolk–shell nanostructures were then recovered using centrifugation and dried under vacuum overnight.

Characterization. SEM and TEM images were taken using a FEI XL30 Sirion SEM (accelerating voltage 5 kV) and a FEI Tecnai G2 F20 X-TWIN (accelerating voltage 200 kV), respectively. Elemental analysis was performed using energy-dispersive X-ray spectroscopy and electron energy loss spectroscopy equipped in the TEM. X-ray diffraction patterns were obtained on a PANalytical X'Pert Diffractometer using Cu Kα radiation. Thermogravimetric analysis was carried out using a Netzsch STA 449 at a heating rate of 2 $^{\circ}C\,min^{-1}$ under argon atmosphere. ICP optical emission spectroscopy was performed using a Thermo Scientific ICAP 6300 Duo View Spectrometer. Nitrogen adsorption data were collected on a Micromeritics ASAP 2020 Analyser after degassing at 180 °C for 12 h.

Electrochemical measurements. To prepare the working electrodes, the various sulphur-based materials were mixed with carbon black (Super P) and polyvinylidene fluoride binder (75:15:10 by weight) in *N*-methyl-2-pyrrolidinone to form a slurry. This slurry was then coated onto aluminium foil using doctor blade and dried under vacuum to form the working electrode. 2032-type coin cells were assembled in an argon-filled glove box using lithium foil as the counter electrode. The electrolyte used was a freshly prepared solution of lithium bis(trifluoromethanesulfonyl)imide (1 M) in 1:1 v/v 1,2-dimethoxyethane and 1,3-DOL containing $LiNO_3$ (1 wt%). Galvanostatic cycling was carried out using a 96-channel battery tester (Arbin Instruments) from 1.7–2.6 V versus Li^+/Li. Specific capacity values were calculated based on the mass of sulphur in the samples, which was determined using thermogravimetric analysis (Supplementary Fig. S6). The sulphur content was found to be ~71 wt% in the yolk–shell nanostructures, accounting for ~53 wt% of the electrode mix, with a typical sulphur mass loading of 0.4–0.6 $mg\,cm^{-2}$.

References

1. Arico, A. S., Bruce, P., Scrosati, B., Tarascon, J. M. & Van Schalkwijk, W. Nanostructured materials for advanced energy conversion and storage devices. *Nat. Mater.* **4,** 366–377 (2005).
2. Bruce, P. G., Freunberger, S. A., Hardwick, L. J. & Tarascon, J.-M. Li-O_2 and Li-S batteries with high energy storage. *Nat. Mater.* **11,** 19–29 (2012).
3. Yang, P. D. & Tarascon, J. M. Towards systems materials engineering. *Nat. Mater.* **11,** 560–563 (2012).
4. Whittingham, M. S. Lithium batteries and cathode materials. *Chem. Rev.* **104,** 4271–4301 (2004).
5. Goodenough, J. B. & Kim, Y. Challenges for rechargeable Li batteries. *Chem. Mater.* **22,** 587–603 (2010).
6. Lee, Y. J. *et al.* Fabricating genetically engineered high-power lithium ion batteries using multiple virus genes. *Science* **324,** 1051–1055 (2009).
7. Kang, B. & Ceder, G. Battery materials for ultrafast charging and discharging. *Nature* **458,** 190–193 (2009).
8. Chung, S. Y., Bloking, J. T. & Chiang, Y. M. Electronically conductive phospho-olivines as lithium storage electrodes. *Nat. Mater.* **1,** 123–128 (2002).
9. Nishizawa, M., Mukai, K., Kuwabata, S., Martin, C. R. & Yoneyama, H. Template synthesis of polypyrrole-coated spinel $LiMn_2O_4$ nanotubules and their properties as cathode active materials for lithium batteries. *J. Electrochem. Soc.* **144,** 1923–1927 (1997).
10. Park, C. M., Kim, J. H., Kim, H. & Sohn, H. J. Li-alloy based anode materials for Li secondary batteries. *Chem. Soc. Rev.* **39,** 3115–3141 (2010).
11. Ji, L. W., Lin, Z., Alcoutlabi, M. & Zhang, X. W. Recent developments in nanostructured anode materials for rechargeable lithium-ion batteries. *Energy Environ. Sci* **4,** 2682–2699 (2011).
12. Kasavajjula, U., Wang, C. & Appleby, A. J. Nano- and bulk-silicon-based insertion anodes for lithium-ion secondary cells. *J. Power Sources* **163,** 1003–1039 (2007).
13. Chan, C. K. *et al.* High-performance lithium battery anodes using silicon nanowires. *Nat. Nanotech.* **3,** 31–35 (2008).
14. Magasinski, A. *et al.* High-performance lithium-ion anodes using a hierarchical bottom-up approach. *Nat. Mater.* **9,** 353–358 (2010).
15. Mikhaylik, Y. V. & Akridge, J. R. Polysulfide shuttle study in the Li/S battery system. *J. Electrochem. Soc.* **151,** A1969–A1976 (2004).
16. Yamin, H., Gorenshtein, A., Penciner, J., Sternberg, Y. & Peled, E. Lithium sulfur battery - oxidation reduction-mechanisms of polysulfides in THF solutions. *J. Electrochem. Soc.* **135,** 1045–1048 (1988).
17. Barchasz, C., Lepretre, J.-C., Alloin, F. & Patoux, S. New insights into the limiting parameters of the Li/S rechargeable cell. *J. Power Sources* **199,** 322–330 (2012).
18. Aurbach, D. *et al.* On the surface chemical aspects of very high energy density, rechargeable Li-sulfur batteries. *J. Electrochem. Soc.* **156,** A694–A702 (2009).
19. Elazari, R., Salitra, G., Garsuch, A., Panchenko, A. & Aurbach, D. Sulfur-impregnated activated carbon fiber cloth as a binder-free cathode for rechargeable Li-S batteries. *Adv. Mater.* **23,** 5641–5644 (2011).
20. Ji, X., Lee, K. T. & Nazar, L. F. A highly ordered nanostructured carbon-sulphur cathode for lithium-sulphur batteries. *Nat. Mater.* **8,** 500–506 (2009).
21. Ji, X., Evers, S., Black, R. & Nazar, L. F. Stabilizing lithium-sulphur cathodes using polysulphide reservoirs. *Nat. Commun.* **2,** 325 (2011).
22. Schuster, J. *et al.* Spherical ordered mesoporous carbon nanoparticles with high porosity for lithium-sulfur batteries. *Angew. Chem. Int. Ed.* **51,** 3591–3595 (2012).
23. Liang, C. D., Dudney, N. J. & Howe, J. Y. Hierarchically structured sulfur/carbon nanocomposite material for high-energy lithium battery. *Chem. Mater.* **21,** 4724–4730 (2009).
24. Yang, Y. *et al.* New nanostructured Li_2S/silicon rechargeable battery with high specific energy. *Nano Lett.* **10,** 1486–1491 (2010).
25. Zheng, G., Yang, Y., Cha, J. J., Hong, S. S. & Cui, Y. Hollow carbon nanofiber-encapsulated sulfur cathodes for high specific capacity rechargeable lithium batteries. *Nano Lett.* **11,** 4462–4467 (2011).
26. Guo, J., Xu, Y. & Wang, C. Sulfur-impregnated disordered carbon nanotubes cathode for lithium-sulfur batteries. *Nano Lett.* **11,** 4288–4294 (2011).
27. Jayaprakash, N., Shen, J., Moganty, S. S., Corona, A. & Archer, L. A. Porous hollow carbon@sulfur composites for high-power lithium-sulfur batteries. *Angew. Chem. Int. Ed.* **50,** 5904–5908 (2011).
28. Wang, H. *et al.* Graphene-wrapped sulfur particles as a rechargeable lithium-sulfur battery cathode material with high capacity and cycling stability. *Nano Lett.* **11,** 2644–2647 (2011).
29. Ji, L. *et al.* Graphene oxide as a sulfur immobilizer in high performance lithium/sulfur cells. *J. Am. Chem. Soc.* **133,** 18522–18525 (2011).
30. Wang, J. L., Yang, J., Xie, J. Y. & Xu, N. X. A novel conductive polymer-sulfur composite cathode material for rechargeable lithium batteries. *Adv. Mater.* **14,** 963–965 (2002).
31. Xiao, L. *et al.* A soft approach to encapsulate sulfur: polyaniline nanotubes for lithium-sulfur batteries with long cycle life. *Adv. Mater.* **24,** 1176–1181 (2012).
32. Wu, F. *et al.* Sulfur/polythiophene with a core/shell structure: synthesis and electrochemical properties of the cathode for rechargeable lithium batteries. *J. Phys. Chem. C* **115,** 6057–6063 (2011).
33. Fu, Y. & Manthiram, A. Core-shell structured sulfur-polypyrrole composite cathodes for lithium-sulfur batteries. *RSC Adv.* **2,** 5927–5929 (2012).
34. Li, X. *et al.* Hollow core-shell structured porous Si-C nanocomposites for Li-ion battery anodes. *J. Mater. Chem.* **22,** 11014–11017 (2012).
35. Su, L., Jing, Y. & Zhou, Z. Li ion battery materials with core-shell nanostructures. *Nanoscale* **3,** 3967–3983 (2011).
36. Zang, L. *et al.* Amorphous microporous titania modified with platinum(IV) chloride - A new type of hybrid photocatalyst for visible light detoxification. *J. Phys. Chem. B* **102,** 10765–10771 (1998).
37. Yan, D., Kai, X., Shizhao, X. & Xiaobin, H. Analysis of polysulfide dissolved in electrolyte in discharge-charge process of Li-S battery. *J. Electrochem. Soc.* **159,** A421–A425 (2012).
38. Yang, Z. *et al.* Nanostructures and lithium electrochemical reactivity of lithium titanites and titanium oxides: a review. *J. Power Sources* **192,** 588–598 (2009).
39. Furukawa, H., Hibino, M. & Honma, I. Electrochemical properties of nanostructured amorphous, sol-gel-synthesized TiO_2/acetylene black composite electrodes. *J. Electrochem. Soc.* **151,** A527–A531 (2004).
40. Evers, S., Yim, T. & Nazar, L. F. Understanding the nature of absorption/adsorption in nanoporous polysulfide sorbents for the Li-S battery. *J. Phys. Chem. C* **116,** 19653–19658 (2012).

Acknowledgements

This work was supported by the Department of Energy, Office of Basic Energy Sciences, Division of Materials Sciences and Engineering, under Contract DE-AC02-76SF00515, through the SLAC National Accelerator Laboratory LDRD project. Z.W.S. and G.Z. acknowledge the support of an A*STAR National Science Scholarship. We thank Ming Gong for help in nitrogen adsorption measurements.

Author contributions

Z.W.S. and Y.C. conceived the idea. Z.W.S. and W.L. carried out material synthesis and electrochemical tests. J.J.C., G.Z., Y.Y., M.T.M. and P.-C.H. performed material characterization. Z.W.S. and Y.C. co-wrote the paper. All the authors discussed the results and commented on the manuscript.

Additional information

Supplementary Information accompanies this paper on http://www.nature.com/naturecommunications

Competing financial interests: The authors declare no competing financial interests.

Reprints and permission information is available online at http://npg.nature.com/reprintsandpermissions/

How to cite this article: Seh, Z. W. *et al.* Sulphur–TiO_2 yolk–shell nanoarchitecture with internal void space for long-cycle lithium–sulphur batteries. *Nat. Commun.* 4:1331 doi: 10.1038/ncomms2327 (2013).